Integrated Approach to Optimization of an Ultrasonic Processor

Vijayanand S. Moholkar and Marijn M. C. G. Warmoeskerken
Textile Technology Group, Dept. of Chemical Engineering, University of Twente, NL- 7500 AE Enschede, The Netherlands

In an ultrasonic processor, the input electrical energy undergoes many transformations before getting converted into the cavitation energy, which is dissipated in the medium to bring out the physical/chemical change. An investigation of the influence of free and dissolved gas content of the system on the efficiency of this energy transformation chain is attempted. The results of the experiments reveal that the cavitation intensity produced in the medium varies significantly with the gas content of the system. A unified physical model, which combines basic theories of acoustics and bubble dynamics, has been used to explain the experimental results. An attempt has been made to establish the mechanism of the steps in the energy transformation chain, the involved physical parameters, and interrelations between them. It has been found that the influence of free and dissolved gas content of the medium on the overall energy transformation occurs through a complex inter-dependence of several parameters. Thus, simultaneous optimization of individual steps in the energy transformation chain, with an integrated approach, is necessary for the optimization of an ultrasonic processor. The present study puts forth a simple methodology, with the gas content of the system as manipulation parameter, for this purpose.

Introduction

Use of ultrasound for various homogeneous and heterogeneous chemical processes, popularly known as *sonochemistry*, is well known. One of the most recent applications of ultrasound is in the intensification of wet-textile processes. The current wet-textile processes suffer from two major drawbacks: low water and energy efficiency, and longer process times. Both of these drawbacks can be overcome by application of ultrasound. In the past few years several articles [for example, McCall et al. (1998); Rathi et al. (1997); Thakore (1990); Yachmenev et al. (1999)] have reported enhancement in the efficiencies of several wet-textile processes, such as washing, rinsing, bleaching, mercerization, with application of ultrasound. Despite the encouraging results of these studies, to date, ultrasound-based wet-textile processes have remained in the laboratory, with little industrial activity, even on a pilot scale. The two major factors that have contributed to this effect are the lack of precise knowledge of the physical mechanism of the ultrasound-enhanced wet-textile processes, and the drawbacks of the ultrasonic reactors, namely, directional sensitivity of the ultrasound effects, the erosion of the sonicator surface, and the nonuniform volumetric energy density at optimum cavitation conditions. It was recently shown by us (Moholkar and Warmoeskerken, 2002; Moholkar, 2002) that transient cavitation in the medium (that is, water) in the close vicinity of the textile surface is the basic physical mechanism of ultrasonic mass-transfer intensification in textiles. However, before the ultrasonic textile processes could be implemented on an industrial scale, it is also necessary to understand the energy mechanism of sonic processors.

In a sonic processor, the electrical energy input is transformed into the cavitation energy, which is dissipated in the system to bring about the physical or chemical change through various steps, as shown in Figure 1. First, the electrical energy is converted to mechanical energy in the form of shape oscillations of the piezoelectric crystal. This mechanical energy is converted into the acoustical energy in the form of ultrasound waves, once the shape oscillations of the piezo-

Correspondence concerning this article should be addressed to V. S. Moholkar.
Current address of V. S. Moholkar: "Karishma", 2/A, Pramod Nagar, Vijapur Road, Solapur-413 004, Maharashtra, India.

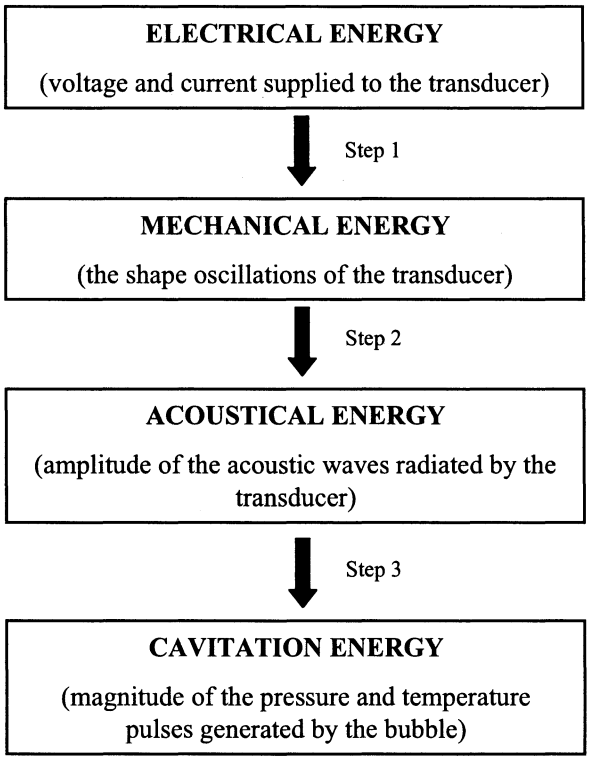

Figure 1. The energy transformation chain in an ultrasonic processor.

electric transducer are coupled to the medium, such as water. The ultrasound energy is then transformed into the cavitation energy through the radial motion of bubbles driven by ultrasound. The high-temperature and -pressure pulses produced during the transient collapse of the bubbles are responsible for bringing out the desired physical or chemical change. As a consequence, the overall energy efficiency of the ultrasonic processor is the product of the individual efficiencies of the discrete steps in the energy transformation chain depicted in Figure 1. Therefore, the optimization of an ultrasonic processor would basically mean simultaneous optimization of all the discrete steps in the energy transformation chain. This necessitates an integrated approach for the optimization of an ultrasonic processor. The present study attempts to present a simple methodology for this purpose using the gas content of the system as a manipulation parameter. We deal with the air–water system in this study and, hence, the word liquid refers to water and the word gas refers to air. The effect of the gas content of the system on a sonochemical process is well known. However, in this article, we have made an attempt to identify the exact mechanism of this influence and the involved physical parameters as the input electrical energy undergoes several transformations before ending up as cavitation energy in the medium. We have demonstrated the effect of variation in both the free and dissolved gas in the medium on the energy transformation chain experimentally using the analysis of the spectral characteristics of the acoustic emission and the power consumption of the ultrasound horn. The results of the experiments have been explained using a unified mathematical model developed on the basis of the equivalent circuit of a piezoelectric transducer. This model includes theory of the impedance tube, the theory of the acoustic-wave propagation in the bubbly liquid, and the theory of rectified diffusion in the oscillating bubbles.

Experimental

Experimental system

Experiments were carried out in a glass cell (Dimensions: ID = 60 mm; OD = 70 mm; height = 80 mm). The cell had a 3-mm-
thick cork rubber lining on the inside wall that acts as an acoustic absorber [reflection coefficient = 0.02; Ensminger (1988)]. This lining helps achieve a unidirectional sound field in the cell by preventing random reflections from the walls of the cell. The cell was mounted on a stainless steel bottom (thickness = 51 mm) that acts as a rigid reflector for the ultrasound waves [reflection coefficient = 0.99; Ensminger (1988)]. For the positioning of the hydrophone at a particular location between the ultrasound horn tip and the rigid reflector, the cell had two screw caps at a distance of 15 mm and 30 mm from the bottom. The ultrasound horn was mounted on the shaft of a laboratory jack and the cell was placed on the base. The jack could be raised or lowered to adjust the distance between the rigid bottom of the cell and the ultrasound horn tip.

The ultrasound unit was composed of a custom-built ultrasound horn with a central resonance frequency of 25 kHz, when vibrating in air. The horn is shown in Figure 2 along with its dimensions. The horn tip has a small circular groove on it, the significance of which is explained in the next sec-

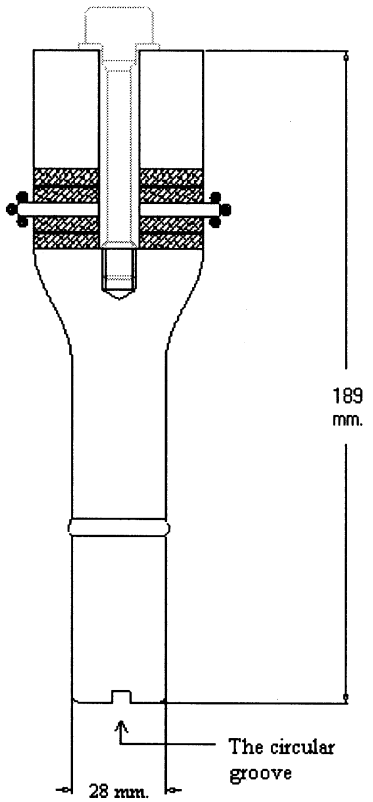

Figure 2. The design of the ultrasound transducer.

tion. The horn also had the facility of cooling the piezoelectric element in order to keep the temperature of the horn constant. The horn was driven by a signal generator (Hewlett-Packard Ltd., Model 3324A) and a radio-frequency amplifier (ENI Inc., Model 2100L). The amplifier had a maximum power output of 200 W for an input impedance of 50 Ω. The power consumption of the ultrasound horn was monitored by measuring the voltage and current supplied to the horn and the phase angle between them. For this purpose, a voltage probe (Tektronics Ltd., Model 6138A) and a current clamp (Farnell Inc., Model PR-20) were used. The measurements of voltage, current, and the phase angle were done on a digital oscilloscope (Tektronics Ltd., Model 430A). For the measurements of the pressure-signals, a small (4-mm) hydrophone supplied by TNO-TPD (Delft, The Netherlands) was used along with a charge amplifier (Nexus Range, Type 2690). This hydrophone was not calibrated, and therefore only relative variation in the cavitation intensity in the medium for different process conditions could be discerned with the pressure-signal measurements made with this hydrophone. The output of this amplifier was fed to the digital oscilloscope. The pressure signals measured on the oscilloscope were transferred to a computer via a GPIB card. The record length of the oscilloscope was set at 30,000 points in 12 divisions with a time scale of 1 ms/div. Thus, the sampling frequency of the pressure signal was 2.5 MHz.

Experimental procedure

The experiments were performed in three sets using water with different saturations of dissolved air as the medium. We used the dissolved oxygen content of the medium as a measure of the dissolved air concentration. The experiments were conducted at 20°C. The saturation concentration of oxygen corresponding to this temperature is 9 ppm. In the first set, demineralized water saturated with the dissolved air was used. In the second set, undersaturated demineralized water was used with dissolved oxygen content reduced to 2 ppm. The method used for degassing water is described in the next subsection. In the third set the same degassed water as in set 2 was used, but in this case the water was left standing undisturbed for about 30 min after degassing. In addition the circular groove in the tip of the horn was filled with silicon rubber. The reasons behind these features of experiment set 3 are explained in the next section. In each set, the cell was filled with 125-mL water. The ultrasound horn was driven at a frequency of 25 kHz with an input of 90 mV_{rms} from the signal generator to the radio-frequency amplifier. It must, however, be noted that the actual power absorbed by the ultrasound horn depends on the impedance of the medium in which the horn is oscillating. The distance between the tip of the horn and the rigid bottom was fixed at 60 mm and the hydrophone was placed at a distance of 30 mm from the bottom of the cell. The rationale behind these distances is explained in the next section. We would like to point out that, since the cell is driven below its cutoff frequency (approximately equal to 40 kHz) the acoustic waves generated in the medium have planar nature. The ultrasound horn was operated intermittently to avoid any significant rise in the temperature of the medium. Since the cavitation is a random phenomenon, 50 pressure signals were collected at one location. The peak-to-peak voltage (V_{p-p}) and peak-to-peak current (I_{p-p}) supplied to the ultrasound horn and the phase angle between them (ϕ) was written down every 30 s. The FFT of the pressure signals measured with the hydrophone was obtained using the MathCad software (version 8.0). The power consumption of the ultrasound horn can be calculated using a simple formula: Power $= (V_{p-p} \times I_{p-p} \times \cos\phi)/4$. The acoustic-pressure amplitude generated by the ultrasound horn can be calculated using the formula: $I = (\eta P_A^2/\rho c)$, where I is the power input to the horn per unit area in a different set of experiments, and η is the transducer efficiency [typically $\sim 40\%$; Shah et al. (1999)].

Method for degassing water

A conventional method for degassing water is to pull vacuum over it. However, by this method it takes a very long time to reach low concentrations of dissolved gas content, as required in this study (2 ppm of dissolved oxygen). Van der Vlist et al. (1994) have reported a chemical method for degassing water that overcomes this shortcoming. Due to this advantage, we have used this method for degassing water described as follows.

Air in 20-L of demineralized water was stripped out using CO_2, bubbling from four circular porous glass slabs mounted at the bottom of the vessel. After 12 min of bubbling the water was transferred to the ultrasound bath. Thereafter, the dissolved CO_2 was converted to carbonate by increasing the pH to a value between 9 and 10 by adding 6 to 7 g of NaOH.

Analysis of Experimental Methodology

In this section we provide justifications for certain methodologies adopted in the experimental section and the choice of certain experimental parameters.

Standing-wave formation in cell

The acoustic waves emitted by the ultrasound horn get reflected from the rigid bottom of the cell. The interference between incident and reflected waves gives rise to a standing wave. In order to determine the pressure amplitude variation between the ultrasound horn tip and the rigid bottom of the cell, we use the theory of standing waves (Pierce, 1989). The properties of standing wave are:

(1) In a standing wave, the velocity and pressure are out of phase by 90°, except at the source of sound. At the sound source, the pressure and velocity are always in phase.

(2) The distance between two consecutive pressure antinodes (or pressure maxima) or two consecutive pressure nodes (or pressure minima) is $\lambda/2$, where λ is the wavelength of ultrasound. The distance between a pressure node and pressure antinode is $\lambda/4$.

(3) For a standing-wave formation due to reflection at a rigid boundary, a pressure antinode (or pressure maxima) exists at the boundary, since velocity at the boundary is zero. On the other hand, for a standing-wave formation due to reflection at a pressure release boundary, a pressure node (or pressure minima) exists at the boundary, since velocity is maximum at the boundary.

Using these standing-wave properties, we can easily identify the locations of pressure node and pressure antinodes in the cell. As mentioned earlier, the distance between the ul-

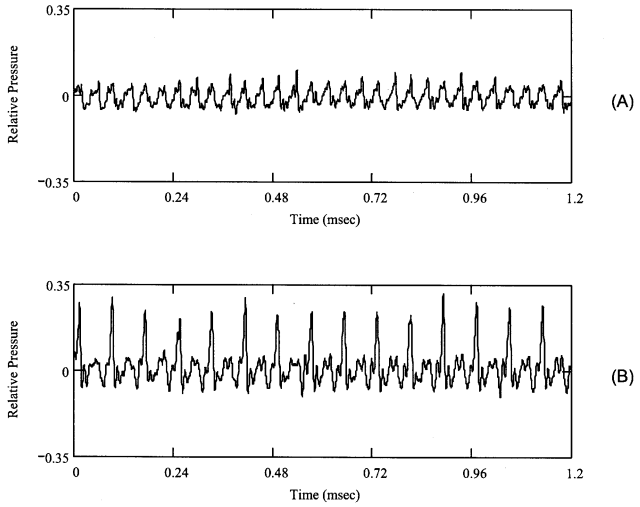

Figure 3. (A) Acoustic pressure signal measured at pressure node; (B) acoustic pressure signal measured at pressure antinode.

Since the hydrophone was not calibrated, it gives only the relative variation in the acoustic pressure signal at pressure node and antinode.

trasound horn tip and the rigid bottom was fixed as 60 mm, which is the wavelength of 25-kHz ultrasound. The bottom of the cell, being rigid, is a pressure antinode, while at the ultrasound horn tip, pressure and velocity are always in phase. In the distance between the rigid bottom and the ultrasound horn tip, the first and second pressure nodes are located at a distance of $\lambda/4$ (15 mm) and $3\lambda/4$ (45 mm) from the bottom. The pressure antinode is located at a distance of $\lambda/2$ from the bottom (or halfway between the ultrasound horn tip and the bottom). In order to confirm the locations of pressure node and antinode, pressure signal measurements were made by placing the hydrophone in the two screw caps of the cell (located at 15 mm and 30 mm from the bottom, as mentioned earlier). The distance between the ultrasound horn tip and the rigid bottom of the cell was adjusted to 60 mm and the horn was driven at 25 kHz with power input of 20 W. Figure 3 shows the pressure signal at the two locations. It could be seen that the amplitude of the pressure signal measured at a distance 30 mm from bottom is far higher than the amplitude of the pressure signal collected at 15 mm. This means that pressure maxima exist at a distance of 30 mm (or $\lambda/2$), while pressure minima exist at a distance of 15 mm (or $\lambda/4$) from the bottom. At the pressure antinode the local pressure amplitude is doubled due to constructive interference between the incident and reflected waves, while at the pressure node, the pressure amplitude is very low due to destructive interference. Due to the large acoustic-pressure amplitude, cavitation activity (which is basically the motion of bubbles driven by the acoustic wave) will be prominent at the location of the pressure antinode. Since the principal aim of this study was to deduce the variation in the cavitation intensity with the gas content of the medium, we have placed the hydrophone for acoustic-pressure signal measurement at the pressure antinode, that is, at a distance of 30 mm from the bottom of the cell.

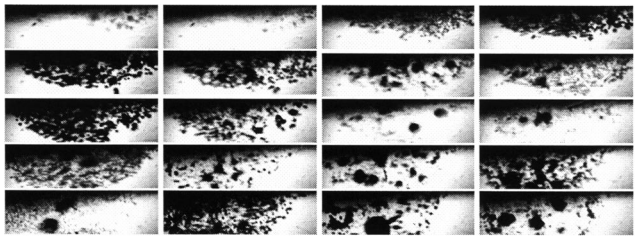

Figure 4. Twenty frames (arranged sequentially left to right in consecutive rows) from a high-speed movie of bubble activity at the tip of the ultrasound horn.

The upper edge of the frames is the tip of the horn. Frame size: 25×12.5 mm. Frame rate: 2,000 f/s. Time interval between frames: 500 μs.

Variation in the gas content of the medium

In the present study, gas existed in two forms in the medium: (1) dissolved gas, and (2) free gas, in the form of free-floating bubbles or in the form of microbubbles trapped in the crevices of the experimental system (that is, the cell and ultrasound horn). These two forms of gases are relatively independent of each other. The free-floating bubbles easily dissolve away in the medium, and hence, the free gas in the medium is mainly contributed by stabilized gas pockets in the crevices of the solid boundaries in the medium. These gas pockets provide nuclei for cavitation in the medium. One of the possible locations for these gas pockets is the circular groove in the tip of the ultrasound horn. As the horn is introduced in the cell, with its tip held parallel to the water surface, all the air in the groove is not replaced by water, thus causing entrapment of some air pockets. In order to confirm air entrapment in the groove in the tip of the horn, a high-speed video recording was done to monitor the nucleation at the tip of the horn. A high-speed camera (Kodak Imager CR 1000; frame rate: 2000 fps) was used for imaging using a dark-field illumination technique for observation of bubble motion. A selection from the series of consecutive frames sampled from the movie is shown in Figure 4. Information about the other parameters is given in the figure caption. The tip of the horn forms the upper edge of the photographic frames. It can be seen that due to nucleation, clouds of bubbles originate and grow at the tip of the horn. Later, they are periodically expelled in water, probably due to Bjerknes forces. Thus, the high-speed photographic record shown in Figure 4 confirms air entrapment in the circular groove in the tip of the horn that provides nuclei for cavitation in the medium.

In experiment set 3, water was left standing for about 30 min. after degassing to 2 ppm of dissolved oxygen. In addition, the circular groove in the tip of the horn was filled with silicon rubber, thus making the horn tip as smooth as possible. High under-saturation of the medium causes dissolution of most of the free-floating bubbles. The smooth horn tip does not entrap any air pockets, and, hence, there is no source of cavitation nuclei in the third set of experiments. Thus, in the third set of experiments, the medium was not only degassed but also denucleated. On the other hand, in experiment set 2, the medium was only degassed. The groove in the

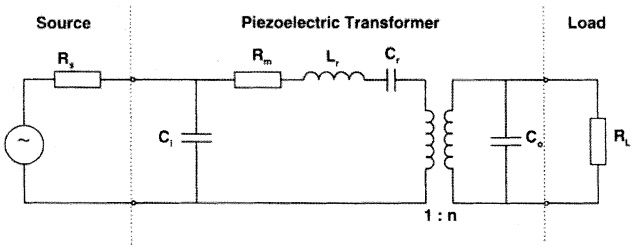

Figure 5. Equivalent circuit of a piezoelectric transducer.

The piezoelectric element is an electrical condenser of capacitance C_0 due to the dielectric nature of the transducer material. Therefore it does not affect the mechanical impedances, namely, R_m, L_r, and C_r. R_s is the source impedance or internal impedance of the electrical power source.

ultrasound horn tip was left unfilled, and, thus, it provided nuclei for cavitation in the medium due to air entrapment.

The Physical Model

Before proceeding to the development of the physical model, we discuss the equivalent circuit of a piezoelectric transducer, which converts electrical energy into ultrasound energy. The electrical characteristics of the transducers are affected by the type of mechanical loading to which they are subjected. Since the influence of the mechanical load has characteristics of the electrical parameters of the transducer, it is useful for the design of a transducer that the mechanical loading parameters are represented by a circuit diagram, which also includes the electrical parameters of the transducers. Such a circuit diagram is called an *equivalent circuit* of a transducer, and is shown in Figure 5. It can be seen that the converted mechanical impedance in the equivalent circuits has four components:

(1) The inductance, L_r, due to the mass of the transducer.

(2) The capacitance, C_r, due to the compliance of the transducer.

(3) The resistance, R_m, due to the losses in the transducer (usually negligible).

(4) The load resistance or radiation impedance (R_L), which is the product of the specific acoustic impedance of the medium in which the transducer vibrates (Z_R) and the area of the transducer.

Out of these, R_m, L_r, and C_r depend upon the material of construction and dimensions of the transducer and, hence, cannot be altered once the transducer is fabricated. However, the fourth component, R_L, is subject to variation according to the conditions of the medium for ultrasound wave propagation. The physical significance of R_L can be described as the resistance to the oscillations of the piezoelectric transducer. According to an analysis of the efficiency of the piezoelectric transducer (Ensminger, 1988), maximum power transfer between the electrical power source and the piezoelectric transducer occurs at resonance conditions, at which the frequency-dependent component of the impedance (that is, the *reactance*) is zero. At resonance, the internal impedance of the electrical power source (R_s) matches the value ($R_m + R_L$), which is the total load impedance. For most piezoelectric transducers, which are good conductors, the value of R_m is quite small. For the transducer used in the present study, R_m is 4 Ω, while the internal impedance of the amplifier is 50 Ω. It should be noted, however, that when $(R_m + R_L) > R_s$, the power transfer to the ultrasound horn drops. For the development of the physical model, we take the specific acoustic impedance of the medium as the basis.

Theory of the impedance tube

Sound radiation within a fluid-filled tube by a snuggly fitting piston on one end and a rigid reflector on the other end is one of the basic models in acoustics research, which is used for the explanations of the basic concepts. The experimental setup used in this study resembles this model to some extent: the circular glass cell with a rigid bottom corresponds to the impedance tube with the ultrasound horn acting as the piston, although the diameters of horn and the cell are not same. The oscillatory motion of the piston, assumed to be driven by an external source, creates sound waves that travel in the positive and negative x-direction in the tube (with the origin, $x = 0$, taken to be the mean position of piston face). Inside the tube, the acoustic field variables, that is, the pressure and the velocity of the waves are written as

$$\frac{p}{\rho c} = U(t - x/c) + W(t + x/c) \tag{1}$$

$$v = U(t - x/c) - W(t + x/c) \tag{2}$$

where the functions U and W need to specified. We assume that the motion of the piston with velocity $V_o \cos(\omega t)$ creates a steady-state acoustic field in the tube. The functions U and W can be written as $U(t) = Re[X \exp(-i\omega t)]$ and $W(t) = Re[Y \exp(-i\omega t)]$ (Pierce, 1989). Equations 1 and 2 are now transformed as

$$\frac{p}{\rho c} = Re\left[e^{-i\omega t}\left(Xe^{ikx} + Ye^{-ikx}\right)\right] \tag{3}$$

$$v = Re\left[e^{-i\omega t}\left(Xe^{ikx} - Ye^{-ikx}\right)\right] \tag{4}$$

The constants X and Y are determined by the boundary conditions at both ends of the tube. These conditions are: at $x = 0$, $\hat{v} = V_o$, and at $x = L$, $\hat{p}/\hat{v} = Z$. Substituting X and Y in Eqs. 3 and 4, and rearranging, we get the relation between the amplitudes of pressure and velocity in the tube as a function of x

$$\hat{p} = \rho c V_o \left[\frac{Z\cos k(L - x) - i\rho\, c \sin k(L - x)}{\rho c \cos kL - iZ \sin kL}\right] \tag{5}$$

where $k = 2\pi/\lambda$ is the wave number. The ratio $\hat{p}/V_o$ is called the specific acoustic impedance, and is basically an analog of Ohm's law, that is, ratio of driving force (acoustic-pressure amplitude) to the velocity of particles or fluid elements in the medium. The specific acoustic impedance at the face of the piston can be determined by substituting $x = 0$ in Eq. 5. The expression for Z_R gets further simplified due to the fact that $Z = 4.5 \times 10^7$ kg/m^2 −s; $\rho c = 1.5 \times 10^6$ kg/m^2

$-$s; and, hence, $|Z/\rho c| \gg 1$ as

$$Z_R = i\rho\, c \cot\left(\frac{2\pi L}{\lambda}\right) \tag{6}$$

It can be seen that Z_R is singular, when $L = \lambda$ (that is, the formation of the standing waves). Nonetheless, in reality for $L = \lambda$ the values of Z_R are very high, but not singular due to various losses (such as viscous losses) or nonidealities in the medium.

The velocity of sound in pure (gas-free) water is 1,500 m/s. If water contains dilute dispersions of gas bubbles, the velocity of sound in the liquid (and hence, the wavelength) grows slower. In this case, Z_R can be calculated by substituting the velocity and wavelength of sound in the bubbly mixture estimated using the theory of acoustic-wave propagation in bubbly liquids.

Acoustic-wave propagation in the bubbly liquids

Acoustic-wave propagation in bubbly liquids has been a subject of both experimental and theoretical investigations in a large amount of the published literature during the past several decades (for example, Foldy, 1945; Carstensen and Foldy, 1947; Silberman, 1952; Fox et al., 1955; Macpharson, 1957; van Wijngaarden, 1968, 1972; Caflisch et al. (1985). The most rigorous model for the linear acoustic-pressure-wave propagation in bubbly liquids was given by Prosperetti and Commander (1989), which was a combination of the averaged equations for the bubbly mixtures given by Caflisch et al. (1985) and the nonlinear formulation for the internal dynamics of the bubble that includes the viscous and thermal damping of the bubbles (Prosperetti et al., 1986).

Here we give only the main results of the analysis of Prosperetti and Commander (1989); for the complete derivation of the equations and their solutions the reader is referred to the original article. The complex sound speed in the mixture is

$$c_m = \frac{\omega}{k_m} = \frac{c}{\sqrt{1 + 4\pi c^2 \int_0^\infty \dfrac{R_o f(R_o)\, dR_o}{\omega_o^2 - \omega^2 + 2ib\omega}}} \tag{7}$$

where k_m is the complex wave number. The general mathematical expression for a sound wave is $P_A \exp[i(\omega t - kx)]$. In order to find the phase velocity of the sound wave and its attenuation, we substitute $(c/c_m) = u - iv$ in this expression. Substitution and simplification gives

$$\exp\left[i(\omega t - k_m x)\right] = \exp\left(-\frac{\omega v}{c} x\right) \exp\left[i\omega\left(t - \frac{u}{c} x\right)\right]. \tag{8}$$

From this expression the phase velocity (V) and the attenuation coefficient (A) for the wave in the gas–liquid mixture are deduced

$$V = \frac{c}{u} \quad \text{and} \quad A = \frac{\omega v}{c} \left[\text{or in decibels} \approx 8.686\left(\frac{\omega v}{c}\right)\right] \tag{9}$$

Assuming that the number density of the bubbles is n_b, and all the bubbles in the gas–liquid mixture have uniform initial or mean radius, R_o, we can simplify Eq. 7 as

$$c_m = \frac{c}{\sqrt{1 + \dfrac{4\pi c^2 n_b R_o}{\omega_o^2 - \omega^2 + 2ib\omega}}} \tag{10}$$

For the bubbles with size smaller than the resonant bubble size corresponding to the ultrasound frequency (in other words, for the case $\omega \ll \omega_o$), the natural oscillation frequency (ω_o) and the damping coefficient (b) are written as

$$\omega_o^2 \approx \frac{P_o}{\rho R_o^2}\left(3\gamma - \frac{2\sigma}{P_o R_o}\right) \tag{11}$$

$$b = \frac{\gamma - 1}{10\gamma}\frac{P_o}{\rho D} + \frac{2\mu}{\rho R_o^2} \tag{12}$$

It can be seen that the V and A for the bubbly mixtures are a function of n_b and R_o. Together n_b and R_o decide the total bubble volume fraction in the liquid denoted as $\beta = 4/3\, \pi n_b R_o^3$.

Cavitation nucleation and bubble dynamics

For cavitation to occur, the medium through which the ultrasound passes must have preexisting seed nuclei from which the bubbles grow. Free-floating bubbles may not always form suitable nuclei for two reasons: first, these bubbles may rise due to buoyancy and escape out of the liquid and, second, if the surrounding liquid is undersaturated, they may dissolve away (Epstein and Plesset, 1950)). The potential candidates for cavitation nuclei will be the gas pockets trapped in the crevices of the solid surface. It is well known that for any gas bubble to be stable, the pressure inside the bubble should be greater than the pressure in the bulk by an amount equal to $2\sigma/R$, which is the surface tension pressure that acts toward the center of the bubble. In case a gas pocket is trapped in the crevice, it may be possible that the radius of the curvature of the bubble is concave, as seen from the liquid, which causes the surface tension to pressure act in the liquid, thus reducing the gas pressure inside the bubble. In this case gas may enter the bubble, thus stabilizing it.

Once exposed to ultrasound, the type of radial motion that the nuclei undergo depends on the characteristics of the acoustic pressure field, such as its frequency and the pressure amplitude. The bubbles can undergo either a stable and small-amplitude nonlinear motion for several acoustic cycles called *stable cavitation*, or it can undergo an explosive growth and a transient collapse called *transient cavitation*, which is a high-energy event. The minimum pressure amplitude required to generate transient cavitation (P_T) is the *Blake threshold*, and is a function of the initial bubble radius as (Leighton, 1994)

$$P_T = P_o + \frac{8\sigma}{9}\sqrt{\frac{3\sigma}{2R_o^3\left(P_o + \dfrac{2\sigma}{R_o}\right)}} \tag{13}$$

Extending this analysis, Apfel (1981) defined the transient cavitation threshold as a function of both the initial bubble radius and the frequency of the acoustic wave:

$$R_o = \frac{0.82}{\omega}\frac{1}{\sqrt{P_T/P_o}}(P_T - P_o)\left[1+\frac{2}{3}\frac{(P_T-P_o)}{P_o}\right]^{1/3} \quad (14)$$

For a typical bubble size distribution of 2–10 μm and frequency range of 20–100 kHz, the minimum value of P_T is approximately 1 bar.

The radial motion of a bubble under the influence of ultrasound can be described by the bubble dynamics equation. Several researchers have proposed different equations to describe the radial motion of a bubble (for example, Rayleigh, 1917; Plesset, 1949; Gilmore, 1952; Keller and Miksis, 1980; Prosperetti et al., 1986; Löfstedt et al., 1993). For simulations, we choose the Gilmore equation based on the Kirkwood-Bethe hypothesis (1942), which states that the shock waves due to a bubble motion are propagated with a velocity equal to the sum of the fluid velocity and sound velocity (Akulichev, 1971). The equation of the radial motion is written as

$$R\left[1-\frac{U}{c}\right]\frac{d^2R}{dt^2}+\frac{3}{2}\left[1-\frac{U}{3c}\right]\left(\frac{dR}{dt}\right)^2=\left[1+\frac{U}{c}\right]H + \frac{U}{c}\left[1+\frac{U}{c}\right]\frac{dH}{dR}, \quad (15)$$

where H is the free enthalpy on the surface of the bubble, and can be derived using equation of state for water

$$P = A\left(\frac{\rho}{\rho_o}\right)^n - B. \quad (16)$$

Here H is expressed as

$$H = \frac{n}{n-1}\frac{A^{1/n}}{\rho_o}\left\{\left[\left(P_o+\frac{2\sigma}{R_o}\right)\left(\frac{R_o}{R}\right)^{3\gamma}-\frac{2\sigma}{R}+B\right]^{(n-1)/n} - [P_\infty + B]^{(n-1)/n}\right\} \quad (17)$$

where P_∞ is the pressure in the bulk liquid away from the bubble boundary that drives the bubble motion and is expressed as

$$P_\infty = P_o - P_A \sin(2\pi f t), \quad (18)$$

and A, B, and n are constants (for water, $A = 3001$ atm, $B = 3000$ atm, and $n = 7$). Based on the hypothesis of Hilgenfeldt et al. (1996), the bubble motion has been assumed to be isothermal by setting γ (polytropic constant of the bubble contents) as 1.

In Eq. 15, c is the velocity of sound, and is a function of the enthalpy

$$c = \left[c_o^2 + (n-1)H\right]^{1/2} \quad (19)$$

where c_o ($=\sqrt{An/\rho_o}$) is the velocity of sound at STP conditions. The amplitude of the acoustic wave radiated by the bubbles at a distance $r \gg R$ (far field) is written as

$$P_s(r,t) = \frac{\rho}{4\pi r}\frac{d^2V_b}{dt^2} = \rho\frac{R}{r}\left[2\left(\frac{dR}{dt}\right)^2 + R\frac{d^2R}{dt^2}\right] \quad (20)$$

The higher the intensity of the collapse of the bubble, the higher is the magnitude of the acoustic wave radiated by the bubble. Therefore, we use the magnitude of P_s as a measure of the cavitation intensity resulting out of the bubble motion. A representative value of r is taken as 10 mm.

Rectified diffusion

The transport of gas and vapor across the bubble wall during the radial motion is an interesting and well-studied phenomenon in acoustic cavitation. As far as the transport of the vapor is concerned, it is usually assumed that in a relatively cold liquid, evaporation and condensation processes are much faster than the bubble dynamics, and hence the bubble interior is always saturated with water vapor. The transport of the gas in and out of the bubble, however, has interesting features. A gas bubble in the liquid will dissolve in the absence of the sound field or any stabilization mechanisms. However, if the bubble is undergoing radial motion under the influence of an acoustic wave, the situation is different. In this case, if the amplitude of the acoustic wave driving the bubble motion exceeds a certain threshold value, the bubble may grow due to the process of slow accumulation of gas. This process is termed as *rectified diffusion*.

The general mathematical formulation of the gas diffusion is given as follows: Consider a gas bubble undergoing radial motion in a liquid with dissolved gas concentration C_o. The dissolved gas transport within a liquid in a spherically symmetric system is described by the diffusion equation

$$\frac{DC}{Dt} \equiv \frac{\partial C}{\partial t} + v_r\frac{\partial C}{\partial r} = D_g\left[\frac{\partial^2 C}{\partial r^2}+\frac{2}{r}\frac{\partial C}{\partial r}\right]. \quad (21)$$

In order to calculate the mass transfer of gas between the liquid and the oscillating bubble, one needs to solve Eq. 21 simultaneously with the bubble dynamics equation. The bubble dynamics equation and the diffusion equation are coupled through the term v_r, and the boundary condition at the bubble wall, which is function of the gas pressure inside the bubble that changes during the radial motion. For an oscillating bubble, the velocity at a distance $r > R(t)$ is: $R^2(dR/dt)/r^2$.

The boundary conditions for Eq. 21 are

$$C(R,t) = C_s P_i(R,t)/P_o \quad \text{and} \quad C(\infty,t) = C_o \quad (22)$$

The mass transported across the bubble wall is

$$\frac{dm_g}{dt} = 4\pi R^2 D_g \frac{\partial C}{\partial r}\bigg|_{r=R(t)} \tag{23}$$

Several researchers during the past few decades have given approximate solutions for mass transport across the bubble for small-amplitude oscillations of the bubble or stable cavitation (Hsieh and Plesset, 1961; Eller and Flynn, 1965; Safar, 1968; Crum, 1984). A general formulation of the rectified diffusion equation is given by Löfstedt et al. (1995) and Fyrillas and Szeri (1996) that can be applied to both small- as well as large-amplitude motion of the bubbles. In our physical model, we have used this formulation to assess the effect of the dissolved gas in the medium on the bubble growth or shrinkage during radial motion. Here we briefly describe the formulation of Fyrillas and Szeri (1996). For more details, the reader should see the original article.

Fyrillas and Szeri (1996) have proposed the idea of treating the problem of rectified diffusion on the basis of separation of time scales. The concentration field in the liquid is split in two parts: first, the oscillatory part $C_{osc}(r, t)$ that changes on a fast time scale T (the period of the acoustic wave), and secondly, a smooth part $C_{smo}(r, t)$ that changes on a slow diffusive time scale $\tilde{t}(=n\tau_D) \gg T$, where τ_D is the diffusive time scale and is defined as R_o^2/D_g. Thus, the total gas concentration in space and time is the sum of the smooth and the oscillatory parts

$$C(r, t) = C_{\text{osc}}(r, t) + C_{\text{smo}}(r, t) \tag{24}$$

After solving the smooth and oscillatory parts of the diffusive problem using singular perturbation analysis, Fyrillas and Szeri show that the oscillatory part's contribution to the mass transport across the bubble wall is negligible. However, the smooth part contributes to the change in the gas content of the bubble. In the asymptotic limit, the smooth profile $C_{smo}(r, \tilde{t})$ converges as

$$\overline{C}_{smo}(h) = C_o + \left[C_s \frac{\langle P_i(t)\rangle_{t,4}}{P_o} - C_o\right] \times \left\{1 - \frac{\int_0^h \frac{dh'}{\langle (3h' + R^3(t))^{4/3}\rangle_{t,0}}}{\int_0^\infty \frac{dh'}{\langle (3h' + R^3(t))^{4/3}\rangle_{t,0}}}\right\}. \tag{25}$$

The growth or shrinkage of the bubble, that is, the change in the mean radius of the bubble (R_o), is calculated from Eq. 23 as

$$\frac{dm_g}{d\tilde{t}} = 4\pi R_o^2 D_g \frac{\partial \overline{C}_{smo}}{\partial r}\bigg|_{r=R} = 4\pi \rho_g R_o^2 \frac{dR_o(\tilde{t})}{d\tilde{t}} \tag{26}$$

$$\frac{\partial \overline{C}_{smo}}{\partial r}\bigg|_{r=R} = \frac{\left[C_o - C_s \frac{\langle P_i(t)\rangle_{t,4}}{P_o}\right]}{\int_0^\infty \frac{dh'}{\langle (3h' + R^3(t))^{4/3}\rangle_{t,0}}} \times \frac{\partial h}{\partial r}\left[\frac{\partial}{\partial h}\left(\int_0^h \frac{dh'}{\langle (3h' + R^3(t))^{4/3}\rangle_{t,0}}\right)\right]_{h=0} = \frac{C_s}{R_o^2(\tilde{t})} \frac{\left[C_o - C_s \frac{\langle P_i(t)\rangle_{t,4}(\tilde{t})}{P_o}\right]}{\int_0^\infty \frac{dh'}{\langle (3h' + R^3(t))^{4/3}\rangle_{t,0}}}. \tag{27}$$

Using Eqs. 26 and 27 the rate of change in the mean radius of the bubble is

$$\frac{d}{d\tilde{t}} R_o(\tilde{t}) = \frac{D_g C_s}{\rho_g R_o^2(\tilde{t})} \frac{\left[C_o - C_s \frac{\langle P_i(t)\rangle_{t,4}(\tilde{t})}{P_o}\right]}{\int_0^\infty \frac{dh'}{\langle (3h' + R^3(t))^{4/3}\rangle_{t,0}}} \tag{28}$$

The time averages (denoted by $\langle \quad \rangle_{t,i}$) in Eqs. 25, 27, and 28 are defined as:

$$\langle f(t)\rangle_{t,i} = \frac{\int_0^T f(t) R^i(t) dt}{\int_0^T R^i(t) dt} \tag{29}$$

The time average of P_i (internal pressure of the bubble) is calculated using the bubble-dynamics equation. The space integral in the denominator of Eq. 28 can be taken $\approx 1/R_{max}$, as a saddle-point approximation (Lohse and Hilgenfeldt, 1997; Löfstedt et al., 1995), where R_{max} is the maximum radius of the bubble during oscillations over one acoustic period. The initial conditions for Eqs. 15 and 17 along with Eq. 28 are $t = 0$, $R = R_o$, $dR/dt = 0$, $C(r, t = 0) = C_o$, with the $C_s = 0.022$ kg·m^{-3} and $D_g \approx 10^{-9}$ m^2·s^{-1}. The values other parameters are $\rho = 1{,}000$ kg·m^{-3}, $\rho_g = 1.2$ kg·m^{-3}, $\sigma = 0.072$ N m, $\mu = 10$ cP, $\gamma = 1.4$, $c = 1{,}500$ m·s^{-1}, $f = 25$ kHz, $P_o = 101{,}325$ Pa, and $L = 60$ mm. Equations 15, 17, and 28 are solved together using the Runge-Kutta fourth-order method with adaptive step-size control (Press et al., 1992).

Results

Experimental results

Three representative acoustic emission spectra (that is, the FFT of the pressure signal measured at pressure antinode) in the first, second, and third sets of experiments are shown in Figure 6A, 6B, and 6C, respectively. The power consumption of the ultrasound horn in different sets of experiments is shown in Figure 6D. The acoustic-emission spectra in different sets of experiments reveal interesting features. In the acoustic-emission spectrum of the first set, in which gassy water was used as the medium, only the peak corresponding to

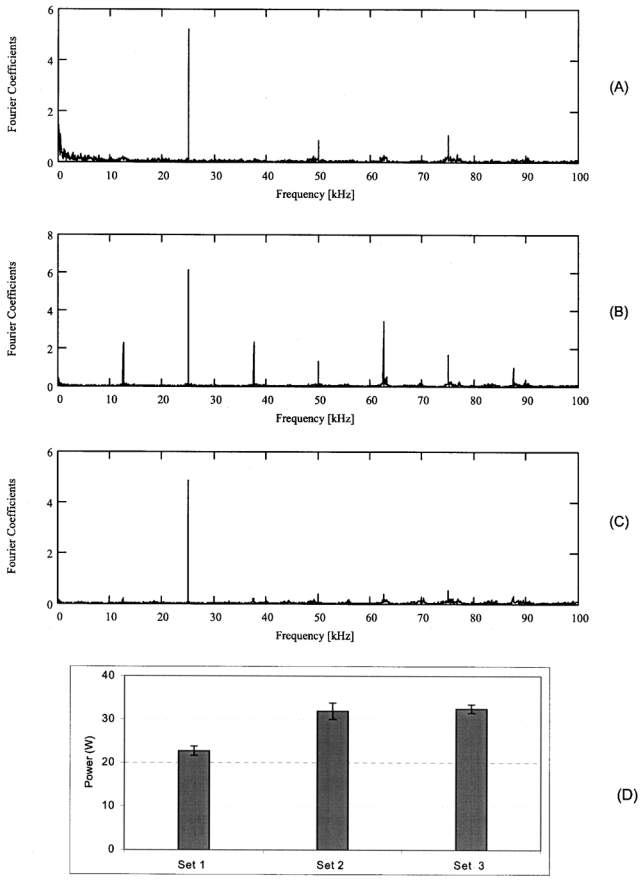

Figure 6. The experimental results: (A) acoustic emission spectrum in experiment set 1; (B) acoustic emission spectra in experiment set 2; (C) acoustic emission spectra in experiment set 3; (D) power consumption of ultrasound horn in different sets of experiments.

the fundamental frequency is prominent, with a weak first harmonic ($2f$) peak. A sharp rise in subharmonic ($f/2$), ultraharmonics ($nf/2$, where $n = 3,5,7, \ldots$) and harmonics (nf, where $n = 2,3,4,...$) is seen in the acoustic-emission spectrum of the second set of experiments. All other frequency components except the fundamental frequency disappear in the acoustic emission spectrum of set 3. We specifically mention that these features of the acoustic-emission spectra were reproducible in the analysis of all the 50 pressure signals measured in each set of experiments. It can be inferred, by comparison of power-consumption values in sets 1 and 2 that the power consumption of the ultrasound horn shows a significant rise with degassing of the medium. However, in addition to degassing, denucleation of the medium does not affect power consumption much, as is evident from power consumption value in set 3, which is almost equal to that in set 2. The pressure amplitudes of the ultrasound wave generated by the medium in three sets of experiment are: set 1 = 0.5 bar, set 2 = 0.8 bar, set 3 = 0.8 bar. It must be pointed out that the pressure amplitude at pressure antinode (where pressure-signal measurements were carried out), in the absence of any attenuating mechanism, is twice the values just mentioned.

Interpretation of acoustic-emission spectrum

The spectral characteristics of the acoustic emission (that is, frequency components present in the spectrum) help detect the kind of radial motion (whether stable or transient) from which the acoustic emission originates. Thus, spectral characteristics of the acoustic-emission are indicative of the cavitation intensity in the medium (Moholkar et al., 2000; Frohly et al., 2000). A detailed analysis of the acoustic-emission spectrum is given by Leighton (1994) and Young (1989). It is generally known that the acoustic cavitation noise spectrum comprises various frequencies related to the fundamental or the driving frequency. These frequencies are either the subharmonic, the ultraharmonic, or the harmonic of the fundamental frequency. The subharmonic component of the acoustic-emission spectrum is of particular interest, because it originates from high-energy transient bubble motion, and thus is a representative of the cavitation intensity in the medium.

Simulation results

For the numerical simulations, we have used representative, yet realistic, values of different physical parameters. An important parameter in the simulations is the initial or mean radius of the bubbles in the medium, which does not have a unique value. Therefore, we make an assumption that the bubble population in the medium is uniform in size, with 10 μm as the mean radius prior to exposure to ultrasound. We have presented the results of numerical simulations in three parts, as described below:

(1) *Trends in specific acoustic impedance (Z_R) and attenuation coefficient (A) as a function of total bubble volume fraction (β) and initial bubble radius (R_o):* Variations in Z_R and A for different values of β and R_o are shown in Figure 7. As written earlier, the relation between β and R_o is $\beta = 4/3\ \pi n_b R_o^3$. It can be inferred from Figure 6 that Z_R is a major function of β and is insensitive to R_o for a given value of β. On the contrary, A is a strong function of R_o for a given value of β. It can be inferred from Figure 7A that a smaller bubble-volume fraction in the medium will result in a large value of specific acoustic impedance. On the basis of the discussion on the equivalent circuit of the piezoelectric transducer presented earlier, one can easily perceive that since $R_m \gg R_s$, a rise in Z_R also increases the power consumption of the ultrasound horn. As mentioned earlier, the amplitude of the ultrasound wave generated by the horn is proportional to the power consumption of the ultrasound horn. Thus, reduction in the bubble-volume fraction in the medium causes an increase in the amplitude of the acoustic wave generated by the ultrasound horn. Low bubble-volume fraction in the medium (for a certain value of R_o) also causes lesser attenuation of the ultrasound wave as it passes through the medium, as indicated by Figure 7B. Thus, overall result of a low bubble-volume fraction is the increase in the acoustic pressure amplitude throughout the medium.

(2) *Growth and shrinkage of the bubbles due to rectified diffusion:* The results of the simulation of the growth and shrinkage of the bubble due to rectified diffusion are shown in Figure 8. It can be inferred from Figure 8A that, for an acoustic pressure amplitude greater than the transient cavitation threshold, the bubbles oscillating in a nearly saturated

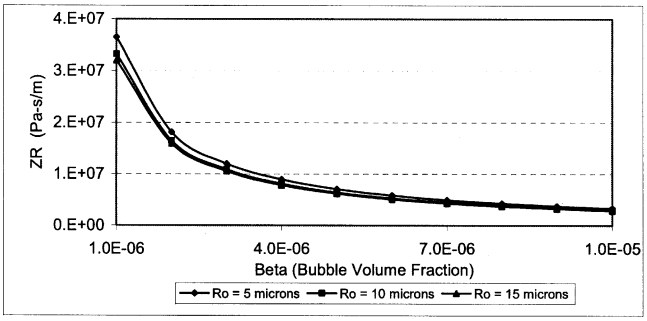

(A)

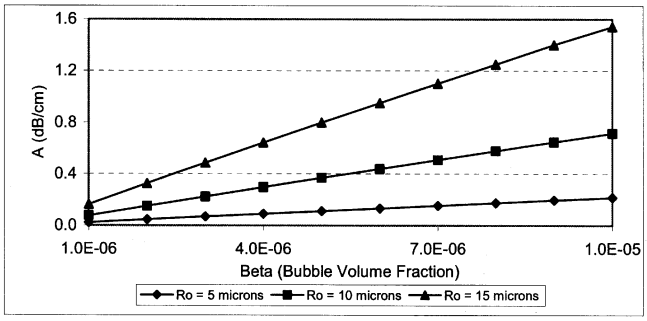

Figure 7. (A) Variation in the specific acoustic impedance of the tube as a function of the bubble volume fraction and the mean radius of the bubbles; (B) variation in the attenuation coefficient of the tube as a function of the bubble volume fraction and the mean radius of the bubbles.

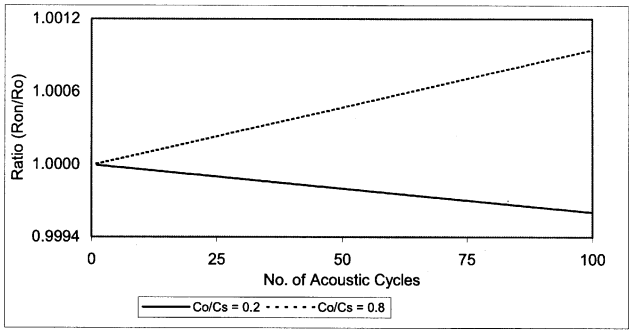

(A)

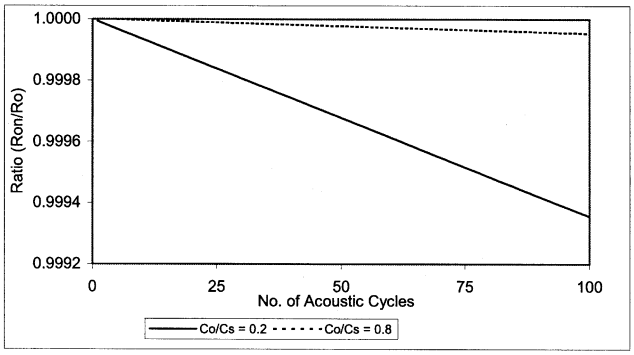

(B)

Figure 8. (A) Growth and dissolution of the air bubbles due to rectified diffusion during radial motion driven by acoustic wave with $P_A > P_T$ in water with different saturations of dissolved air; main parameters for simulations: $R_o = 10$ μm, $P_A = 1.3$ bar, $f = 25$ kHz; (B) dissolution of the air bubbles due to rectified diffusion during radial motion driven by acoustic wave with $P_A < P_T$ in water with different saturations of dissolved air; main parameters for simulations: $R_o = 10$ μm, $P_A = 0.8$ bar, $f = 25$ kHz.

medium ($C_o/C_s = 0.8$) grow, while the bubbles in a highly unsaturated medium ($C_o/C_s = 0.2$) shrink. On the other hand, Figure 8B shows that, for acoustic-pressure amplitudes less than the transient cavitation threshold, the bubbles shrink during oscillations, irrespective of the saturation of the medium. At this point, we must mention that although the percentage change in the mean bubble radius over 100 acoustic cycles is quite small, as shown in Figure 8, the bubble undergoes significant growth or shrinkage in an irradiation period as short as 1 s, which is equivalent to 25,000 acoustic cycles for 25 kHz ultrasound. Growth or shrinkage of the bubbles also causes the bubble-volume fraction in the medium to change (which is basically the product of the volume of a bubble and the total number of bubbles, as mentioned earlier). Thus, the process of rectified diffusion indirectly affects Z_R and A (which, as mentioned in the preceding subsection, are a major function of β and R_o), hence the acoustic-pressure amplitude in the medium.

(3) *Radial motion of the bubbles:* The simulations of the radial motion of the bubbles of different mean radii driven by ultrasound waves with pressure amplitudes (P_A) above and below the transient cavitation threshold (P_T) are shown in Figures 9 and 10, respectively. As mentioned earlier, we have taken an initial mean bubble radius of 10 μm as the basis for simulations. Figure 9 depicts the radial dynamics of the bubbles of sizes 5, 10, and 15 μm. These sizes are selected by taking the growth or shrinkage of a 10-μm bubble into consideration, when oscillating in a medium with a different saturation of dissolved gas. Again, these sizes are selected to represent the shrinkage of the bubble during oscillations. Figure 9 indicates that the pressure amplitude of the acoustic wave radiated by the bubbles reduces after growth (from 10 μm to 15 μm) or shrinkage (from 10 μm to 5 μm) of the bubble. Thus, for the case $P_A > P_T$, P_s has an optimum with the mean radius of the bubble. As far as the other case is concerned, that is, $P_A < P_T$, the pressure amplitude of the acoustic wave radiated by the bubble decreases with the shrinkage of the bubble, as shown in Figure 10. In addition, the pressure amplitudes of radiated acoustic waves are quite small in this case. We can conclude from simulations shown in Figures 9 and 10 that P_s is an increasing function of P_A. However, P_s is an indicator of the cavitation intensity in the medium, as stated earlier. Thus, the cavitation intensity in the medium is also an increasing function of P_A.

We now mention that the bubble motions shown in Figures 9 and 10 are of a different kind. As stated earlier, in transient cavitation the bubble undergoes an explosive growth to several times its initial size, followed by a violent collapse.

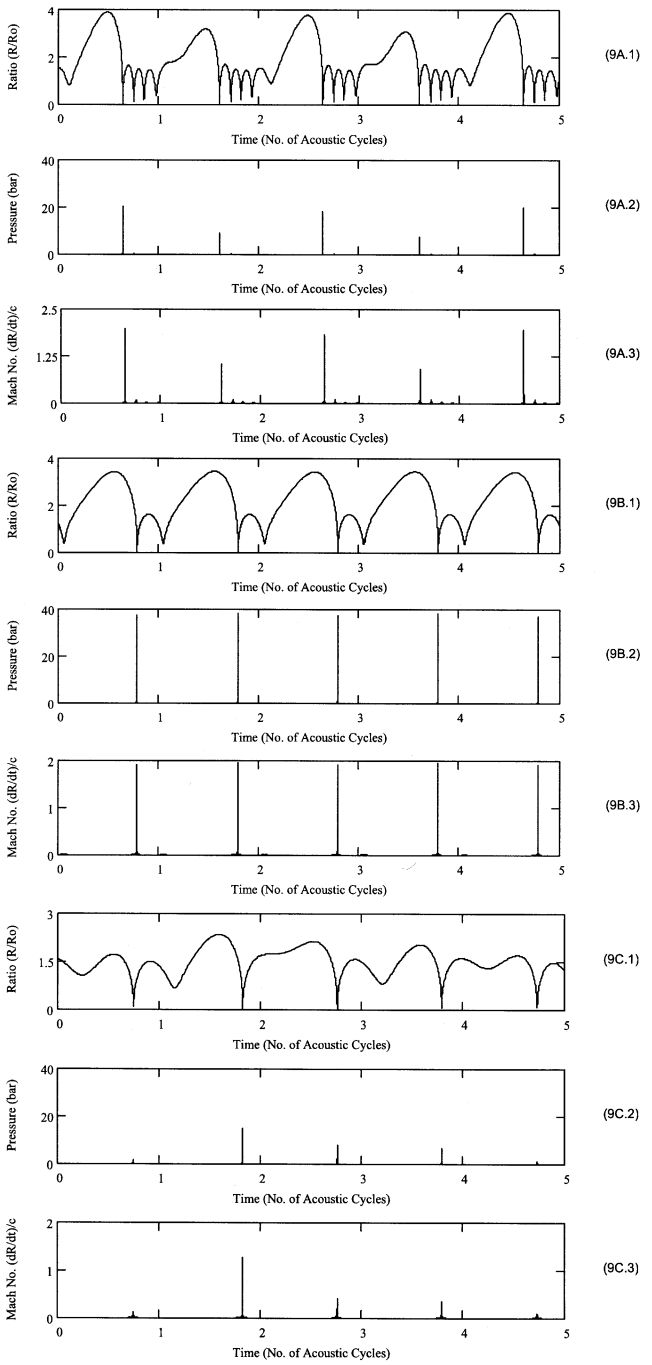

Figure 9. Simulations of the radial motion and sound emission from the bubble of different mean radii driven by acoustic wave with $P_A > P_T$.

Parameters for simulations: (9A) $R_o = 5$ μm, (9B) $R_o = 10$ μm, (9C) $R_o = 15$ μm. Other simulations parameters: $P_A = 1.3$ bar, $f = 25$ kHz. In each of Figures 9A, 9B, and 9C, the first part shows radial motion of the bubble, the second part shows the sound emission during the radial motion, and the third part depicts the variation in bubble wall Mach number during radial motion.

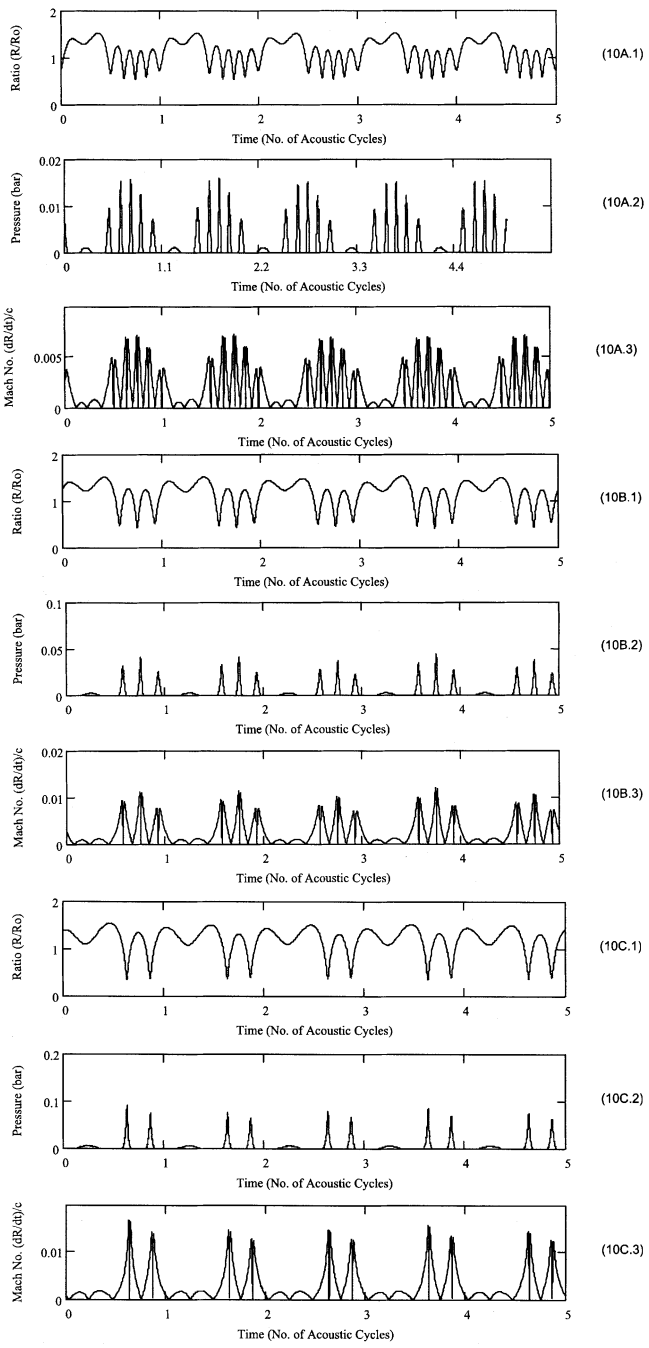

Figure 10. Simulations of the radial motion and sound emission from the bubble of different mean radii driven by acoustic wave with $P_A < P_T$.

Parameters for simulations: (10A) $R_o = 5$ μm, (10B) $R_o = 7.5$ μm, (10C) $R_o = 10$ μm. Other simulations parameters: $P_A = 0.8$ bar, $f = 25$ kHz. In each of the figures 10A, 10B, and 10C, the first part shows radial motion of the bubble, the second part shows the sound emission during the radial motion, and the third part depicts the variation in bubble wall Mach number during radial motion.

Irregularities can develop in the shape of the bubble toward the end of the violent collapse. The source of these irregularities could be proximity of a solid surface, or of other bubbles. Due to these irregularities, the bubble may undergo fragmentation, which is also termed *bubble collapse*. However, if the bubble is isolated, it rebounds after the first compression, retaining its spherical geometry, and repeats the same kind of motion in each acoustic cycle. This kind of mo-

tion is called *repetitive transient cavitation* or *high-energy stable cavitation.* It is a high-energy event because during each transient collapse, the bubble generates extremes of temperature and pressure. An example of this kind of bubble motion is the well-known single-bubble sonoluminescence (Gaitan et al., 1992). The bubble-dynamics equation used in the present study assumes that the bubble is isolated, and remains spherical at all times, in an infinite liquid. Thus, this equation does not take into consideration the previously-mentioned effects that influence the bubble motion. Thus, Figures 9 and 10 show a steady-state solution of the bubble-dynamics equation, where the bubble repeats its motion in each acoustic cycle. Whether the bubble motion is stable or transient can be found by two means: first, the expansion ratio of the bubble during growth, and second, the bubble-wall Mach number during collapse. Flynn (1975a, 1975b) has calculated that if a bubble expands to more than twice its initial size during growth, the subsequent collapse is dominated by inertial forces. In this case, the spherical convergence of the surrounding liquid during the compression phase transfers an increasing amount of kinetic energy to the bubble, which results in energy focusing. Alternatively, if the bubble-wall velocity exceeds the velocity of sound in the medium during compression, the bubble motion is considered to be transient. Several researchers have used the latter criterion for designating bubble motion as transient (for example, Naidu et al., 1993). On the basis of these criteria, one can easily perceive that the radial motion of bubbles depicted in Figure 10 is a case of stable cavitation, while the bubble motion shown in Figure 9 is a case of repetitive transient cavitation.

The extent of interaction between bubbles during radial motion depends on the bubble population in the medium. Cavitation phenomena can also be modeled by considering a cluster of bubbles, instead of a single, isolated bubble. Mørch and coworkers (Hansson and Mørch, 1980; Hansson et al., 1982; Mørch, 1982) have presented equations for the motion of spherical and hemispherical bubble clusters using the continuum mixture model of van Wijngaarden (1968, 1972) as the basis. However, the major shortcoming of this approach is in terms of the shape of the bubble cluster. In reality the bubble cluster can have any shape. Therefore, even with the bubble-cluster equation, one can predict only the trends in the results, which is the case in the single-bubble approach that we have adopted in the present study. In addition, in this work we wanted to demonstrate the effect of the gas content on the energy transformation chain on a broader basis, and hence, we have not incorporated such complications in our analysis.

Discussion

The simulations results presented in the previous section help analyze the experimental results in different sets of experiments.

Analysis of Experimental Results in Set 1. In set 1, saturated (or nondegassed) water was used as the medium. In this case, the nuclei for cavitation are contributed by both the medium and the air pockets trapped in the groove in the ultrasound horn tip. Therefore, the total bubble volume fraction in the medium is high. This results in low specific acoustic impedance, and hence, low power consumption by the ultrasound horn. Thus, the pressure amplitude of the ultrasound wave emitted by the ultrasound horn is small. Another effect of a large bubble population in the medium is the large attenuation of ultrasound waves as they pass through the medium. One can easily perceive that due to the attenuation of ultrasound waves, the acoustic pressure amplitude that a bubble, located away from the ultrasound horn, experiences (P_{Ae}) is smaller than the pressure amplitude at the ultrasound horn tip (P_A). However, experimental techniques used in this study do not have the capacity of distinguishing between P_A and P_{Ae}. Due to the large attenuation of ultrasound waves, it is very likely that the overall acoustic pressure amplitude throughout the medium is lesser than the transient cavitation threshold. Therefore, bubbles in the medium undergo little amplitude oscillatory motion, that is, have stable cavitation. In addition, since the medium is saturated, these bubbles will shrink during oscillations and will dissolve away (as shown in Figure 8B). As a result, the cavitation intensity in the medium is quite low, which is indicated by the absence of a subharmonic peak in the acoustic emission spectrum of set 1. Thus, one can reach the broad conclusion that the efficiency of energy transformation in set 1 is low.

Analysis of Experimental Results in Set 2. In set 2, highly undersaturated water was used as the medium. Degassing of the medium causes reduction in both the free and dissolved gas content of the medium, and as a result, there was a drastic reduction in the bubble population in the medium. The nuclei for cavitation were contributed only by the air pockets trapped in the groove in the ultrasound horn tip. Small bubble-volume fraction in the medium increases the specific acoustic impedance, which, in turn, results in a rise in the power consumed by the horn. Thus, the pressure amplitude of the ultrasound wave generated by the ultrasound horn increases. In addition, due to the low bubble population in the medium, the attenuation of ultrasound waves during their passage through the medium is small. Consequently, the overall acoustic pressure amplitude in the medium is high; conceivably greater than the transient cavitation threshold. Therefore, the bubbles in the medium undergo large-amplitude transient motion that gives rise to strong subharmonic, ultraharmonic and harmonic emission, as seen in the acoustic emission spectrum of set 2. However, during radial motion the bubble would tend to dissolve due to the rectified diffusion (as a result of low saturation of the medium and an acoustic-pressure amplitude that is greater than the transient cavitation threshold, as shown in Figure 8A). For this reason, the cavitation intensity in set 2 is theoretically expected to decrease over a longer period of ultrasound irradiation. Since the experiments in the present study were conducted only for a short duration, this effect was not observed. From this discussion, one can broadly conclude that the total energy transformation efficiency in set 2 is quite high.

Analysis of Experimental Results in set 3. In set 3, the medium was not only degassed, but also denucleated. This means that the bubble-volume fraction in the medium is practically zero. In this case, as written earlier, the specific acoustic impedance of the medium tends to infinity (as indicated by Eq. 6, for condition $L = \lambda$). However, the nonlinearity of the medium and losses in the medium (such as viscous dissipation) cause Z_R to be large, yet finite. Due to high

specific acoustic impedance, the power consumption of the ultrasound horn is high, and thus, the acoustic wave emitted by the ultrasound horn has a large pressure amplitude. The attenuation of the ultrasound waves is also negligible, due to zero bubble-volume fraction in the medium, and, hence, the overall acoustic-pressure amplitude in the medium is greater than the transient cavitation threshold. Despite conditions favoring transient cavitation, no cavitation occurs in the medium due to the lack of proper nuclei for cavitation. Therefore the acoustic-emission spectrum of set 3 shows only one peak, corresponding to the fundamental or the ultrasound frequency. All other peaks indicative of cavitation phenomena in the medium are absent. Thus, one can conclude that the energy transformation efficiency in set 3 is zero, because the acoustical energy introduced in the medium does not get transformed to cavitation energy due to lack of nuclei for cavitation.

We can draw an interesting conclusion from a comparison of the power consumption of the ultrasound horn in set 2 and that in set 3. As shown in Figure 6D, the power consumption of the ultrasound horn in sets 2 and 3 is almost same. In the case of set 2, where the medium was degassed but not denucleated, the value of the bubble volume fraction in the medium is quite small ($<10^{-5}$ or so), while in set 3 the bubble volume fraction in the medium was zero. Despite this difference, identical values of power consumption in sets 2 and 3 indicate that for low values of bubble-volume fraction the specific acoustic impedance is almost independent of the bubble-volume fraction. Justification for this can be made in terms of the effect of gas content on the velocity (c) and wavelength of sound (λ) in water on which the specific acoustic impedance depends, as indicated by Eq. 6. For the bubble-volume fraction of 10^{-6}, c = 1,491 m/s and λ = 59.6 mm, while for gas-free water, c = 1,500 m/s and λ = 60 mm. Thus, the values of c and λ for gas-free water change only slightly when there are bubbles present in the medium, provided that the bubble-volume fraction is small. Thus, the values of the specific acoustic impedance, and hence, the power consumption in sets 2 and 3, was almost the same.

Overview. Analysis of the experimental results in the different sets of experiments reveals that the energy transformation efficiency is highest in set 2 and lowest in set 3. An analysis of the experimental results reveals that the bubble-volume fraction in the medium (or free gas of the medium) and the saturation of the medium (or gas dissolved in the medium) influence the efficiency of the discrete steps in the energy transformation chain, and thus the resultant cavitation intensity in the medium through three parameters:

(1) Specific acoustic impedance (Z_R);
(2) Attenuation coefficient (A);
(3) Acoustic pressure amplitude (P_A).

However, the following interesting conclusion can be drawn from the experimental and simulations results: The effect of free and dissolved gas content on these three parameters is counterproductive. For example, for a given value of dissolved gas content of the medium, P_A affects R_o through the process of rectified diffusion, while R_o affects P_A through the process of attenuation. Additionally, for a given value of the bubble number density, R_o also affects P_A through a specific acoustic impedance, which is a function of the bubble-volume fraction ($\beta = 4/3\pi n_b R_o^3$, as written earlier). The complete nature of the interaction between parameters n_b, R_o, P_A, C_o, A, and Z_R and the resultant cavitation intensity in the medium, which can be worked out from the results and analysis presented earlier, is shown in Figure 11.

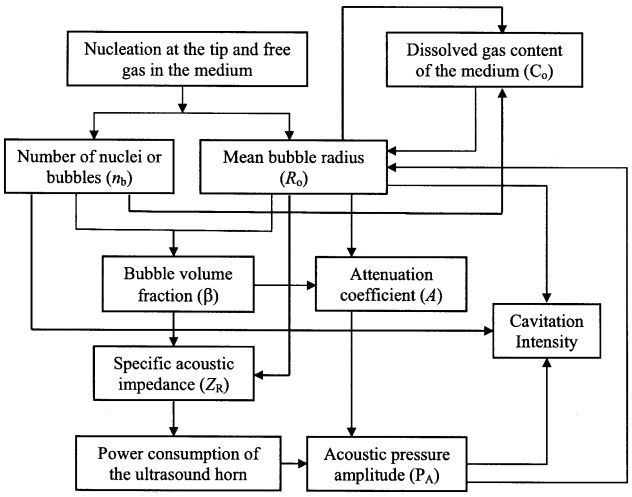

Figure 11. Inter-relations between various parameters that affect the energy transformation in an ultrasonic processor, and thus, the cavitation intensity produced in it.

Conclusion

The results of this study not only shed light on the influence of free and dissolved gas content of the medium on the energy transformation in an ultrasonic processor, but also demonstrate the complex interdependence of various parameters as the input electrical energy passes through a series of transformations, finally ending up as cavitation energy. The set of process parameters values in set 2 (undersaturated medium, C_o/C_s = 0.2, with a very small number density of nuclei) is the best possible combination for achieving the highest efficiency of energy transformation. On the basis of the simulation and experimental results, the nature of the influence of free and dissolved gas content of the medium on the discrete steps in energy transformation can be described as follows:

Step 1. Through the change in specific acoustic impedance, which affects the power consumption of the ultrasound horn and the pressure amplitude of the acoustic wave generated by the ultrasound horn.

Step 2. Via change in the attenuation coefficient, which affects the local acoustic-pressure amplitude in the medium, away from the horn.

Step 3. Through the radial motion of the bubble and energy focusing arising out of it.

An important conclusion of this study is that, since the conversion process of electrical energy to cavitation energy has an overall effect of several highly interdependent parameters, an "integrated" approach is necessary for the optimization of the ultrasonic processor. This approach should take into consideration the primary and secondary influences of different parameters on each other. Basically, this article gives

a qualitative picture of the energy transformation in an ultrasonic processor, which strongly depends on the total bubble-volume fraction in the medium and the dissolved gas concentration. The efficiency of each step, and hence the overall efficiency, can be quantified if the precise values of these parameters are known. As far as the latter parameter (that is, dissolved gas concentration) is concerned, the experimenter can adjust it to its precise value. However, the former parameter (that is, the bubble volume fraction in the medium, which depends on the number of bubbles and their size distribution), is neither easily controllable nor measurable. In addition, this parameter also changes continuously during ultrasound irradiation as a result of bubble fragmentation and the growth/shrinkage of the bubbles due to rectified diffusion. This inherent difficulty keeps us from quantifying the efficiency in each step in the energy transformation chain. Indeed, the lack of knowledge of the number and size distribution of the bubbles is a major problem in the sonochemistry research, and all of the models for sonochemical reactions are based on a single bubble, and so predict the trends in sonochemical yields but do not quantify them.

One of the major shortcomings of the ultrasound processor is the lack of precise knowledge of the mechanism of energy transformation, and this article attempts to deal with this deficiency. We expect that this study will provide basic mechanistic guidelines for optimizing a large-scale ultrasonic processor for any physical or chemical application.

Acknowledgment

The authors acknowledge the funding of Stork Brabant B.V. (Boxmeer, The Netherlands) for the project. The authors also acknowledge TNO-TPD for supplying the hydrophone. The authors are grateful to Prof. Andrea Prosperetti and Dr. Sascha Hilgenfeldt (Physics of Fluids Group, Department of Applied Physics, University of Twente) for their help in this study.

Notation

A = attenuation coefficient of the bubble cloud, $dB \cdot s^{-1}$
b = damping constant, s^{-1}
c = velocity of sound in liquid free of gas, $m \cdot s^{-1}$
c_m = complex velocity of the sound in gas–liquid mixture, $m \cdot s^{-1}$
C_o = dissolved gas concentration in the liquid, $kg \cdot m^{-3}$
c_o = the velocity of sound at the STP conditions, $m \cdot s^{-1}$
C_s = saturation gas concentration in the liquid, $kg \cdot m^{-3}$
D = thermal gas diffusivity, $m^2 \cdot s^{-1}$
D_g = diffusion coefficient of gas, $m^2 \cdot s^{-1}$
H = ethalpy at the bubble surface, J kg^{-1}
k = wave number of liquid, m^{-1}
k_m = complex wave number of gas–liquid mixture, m^{-1}
L = length of the tube, m
m_g = mass of gas in the bubble, kg
n_b = number density of the bubbles, m^{-3}
$\hat{p}$ = complex pressure amplitude of the acoustic wave, Pa
p = pressure in the acoustic wave, Pa
P = pressure, Pa
P_∞ = the pressure in the liquid away from the bubble surface, Pa
P_A = pressure amplitude of the acoustic wave, Pa
P_{Ae} = amplitude of the acoustic wave "experienced" by the bubble, Pa
P_i = internal bubble pressure, Pa
P_o = ambient pressure, Pa
P_s = amplitude of the sound radiated by the bubble, Pa
P_T = transient cavitation threshold, Pa
r = distance from the bubble center, m
R = radius of the bubble, m
$R_{\max}$ = maximum bubble radius during oscillation in one acoustic period, m
R_{no} = the "new" mean bubble radius (after growth or shrinkage from mean radius, R_o), m^{-1}
R_o = initial or mean radius of the bubbles, m
R_L = the radiation impedance for the piezoeletric transducer, N-s $\cdot m^{-1}$
T = period of the acoustic wave driving bubble motion, s
U = the bubble wall velocity (dR/dt), $m \cdot s^{-1}$
$\hat{V}$ = phase speed of sound in gas-liquid mixture, $m \cdot s^{-1}$
$\hat{v}$ = complex velocity amplitude of the acoustic wave, $m \cdot s^{-1}$
v = velocity in the acoustic wave, $m \cdot s^{-1}$
V_b = volume of the bubble, m^3
V_o = amplitude of the oscillatory velocity of the piston, $m \cdot s^{-1}$
Z = specific acoustic impedance of the rigid reflector, Pa-s $\cdot m^{-1}$
Z_R = specific acoustic impedance at the piston (or ultrasound horn) tip, Pa-s $\cdot m^{-1}$

Greek letters

β = bubble volume fraction in the liquid
λ = wavelength of sound, m
σ = surface tension of the liquid, N $\cdot$ m
ρ = density of the liquid, $kg \cdot m^{-3}$
ρ_o = density of the liquid in undisturbed state, $kg \cdot m^{-3}$
ρ_g = density of the gas, $kg \cdot m^{-3}$
ω = angular frequency of sound, s^{-1}
ω_o = natural oscillation frequency of the bubble, s^{-1}
γ = ratio of specific heats of gas
μ = viscosity of the liquid, $kg \cdot m^{-1} \cdot s^{-1}$
τ_D = diffusive time scale, s

Literature Cited

Akulichev, V. A., "Pulsations of Cavitation Voids," *High Intensity Ultrasonic Fields*, L. D. Rosenberg ed., Plenum Press, New York (1971).

Apfel, R. E., *Methods in Experimental Physics*, Vol. 19, P. D. Edmonds, ed., Academic Press, New York, p. 355 (1981).

Caflisch, R. E., M. J. Miksis, G. C. Papanicolaou, and L. Ting, "Effective Equations for Wave Propagation in Bubbly Liquids," *J. Fluid Mech.*, **153**, 259 (1985).

Carstensen, E. L., and L. L. Foldy, "Propagation of Sound Through a Liquid Containing Bubbles," *J. Acoust. Soc. Amer.*, **19**, 481 (1947).

Crum, L. A., "Rectified Diffusion," *Ultrasonics*, **22**, 215 (1984).

Eller, A. I., and H. G. Flynn, "Rectified Diffusion Through Non-Linear Pulsations of Cavitation Bubbles," *J. Acoust. Soc. Amer.*, **37**, 493 (1965).

Ensminger, D., *Ultrasonics: Fundamentals, Technology, Applications*, Dekker, New York, p. 139 (1988).

Epstein, P. S., and M. S. Plesset, "On the Stability of Gas Bubbles in Liquid-Gas Solutions," *J. Chem. Phys.*, **18**(11), 1505 (1950).

Flynn, H. G., "Physics of Acoustic Cavitation in Liquids," *Physical Acoustics*, Vol. IB, W. P. Mason, ed., Academic Press, New York (1964).

Flynn, H. G., "Cavitation Dynamics I. A Mathematical Formulation," *J. Acoust. Soc. Amer.*, **57**, 1379 (1975a).

Flynn, H. G., "Cavitation Dynamics II. Free Pulsations and Models for Cavitation Bubbles," *J. Acoust. Soc. Amer.*, **58**, 1160 (1975b).

Foldy, L. L., "The Multiple Scattering of Waves," *Phys. Rev.*, **67**, 107 (1945).

Fox, F. E., S. R. Curley, and G. S. Larson, "Phase Velocity and Absorption Measurements in Water Containing Air Bubbles," *J. Acoust. Soc. Amer.*, **27**, 534 (1955).

Frohly, J., S. Labouret, C. Bruneel, I. Looten-Baquet, and R. Torguet, "Ultrasonic Cavitation Monitoring by Acoustic Noise Power Measurement," *J. Acoust. Soc. Amer.*, **108**(5), 2012 (2000).

Fyrillas, M., and A. J. Szeri, "Dissolution or Growth of Soluble Spherical Oscillating Gas Bubbles," *J. Fluid Mech.*, **277**, 381 (1994).

Gaitan, D. F., L. A. Crum, C. C. Church, and R. A. Roy, "An Experimental Investigation of Acoustic Cavitation and Sonoluminescence from a Single Bubble," *J. Acoust. Soc. Amer.*, **91**, 3166 (1992).

Gilmore, F. R., *Hydrodynamic Laboratory Report*, Vol. 26-4 California Institute of Technology, Pasadena (1952).

Hansson, I., V. Kedrinskii, and K. A. Mørch, "On the Dynamics of Cavity Clusters," *J. Appl. Phys. (Appl. Phys.)*, **15**, 1725 (1982).

Hansson, I., and K. A. Mørch, "The Dynamics of Cavity Clusters in Ultrasonic (vibratory) Cavitation Erosion," *J. Appl. Phys.*, **51**(9), 4651 (1980).
Hilgenfeldt, S., D. Lohse, and M. P. Brenner, "Phase Diagrams for Sonoluminescing Bubbles," *Phys. Fluids*, **8**(11), 2808 (1996).
Hsieh, D. Y., and M. S. Plesset, "Theory of Rectified Diffusion of Mass Into Gas Bubbles," *J. Acoust. Soc. Amer.*, **33**, 206 (1961).
Keller, J. B., and M. J. Miksis, "Bubble Oscillations of Large Amplitude," *J. Acoust. Soc. Amer.*, **68**, 628 (1980).
Kirkwood, J. B., and H. A. Bethe, Vol. 558, *Office of Science Research and Development Report*, Vol. 558, Washington, DC (1942).
Leighton, T. G., *The Acoustic Bubble*, Academic Press, London (1994).
Löfstedt, R., B. P. Barber, and S. J. Putterman, "Toward a Hydrodynamic Theory of Sonoluminescence," *Phys. Fluids A*, **5**, 2911 (1993).
Löfstedt, R., K. Weninger, S. J. Putterman, and B. P. Barber, "Sonoluminescing Bubbles and Mass Diffusion," *Phys. Rev. E*, **51**, 4400 (1995).
Lohse, D., and S. Hilgenfeldt, "Inert Gas Accumulation in Sonoluminescing Bubbles," *J. Chem. Phys.*, **107**, 6986 (1997).
Macpharson, J. D., "The Effect of Gas Bubbles on Sound Propagation in Water," *Proc. Phys. Soc. Lond. Sec. B*, **70**, 85 (1957).
McCall, R. E., E. R. Lee, G. N. Mock, and P. L. Grady, "Improving Dye Yields of Vats on Cotton Fabric Using Ultrasound," *AATCC Book of Papers*, Amer. Assoc. Textile Chemists and Colorists, p. 188 (1998).
Moholkar, V. S., S. P. Sable, and A. B. Pandit, "Mapping the Cavitation Intensity in an Ultrasound Bath Using Acoustic Emission," *AIChE J.*, **46**(4), 684 (2000).
Moholkar, V. S., and M. M. C. G. Warmoeskerken, "Mechanistic Aspects and Optimization of Ultrasonic Washing," *AATCC Rev.*, **2**(2), 34 (2002).
Moholkar, V. S., *Intensification of Textile Treatments: Sonoprocess Engineering*, Twente Univ. Press, Enschede, The Netherlands (2002).
Mørch, K. A., "Energy Considerations on the Collapse of Cavity Clusters," *Appl. Sci. Res.*, **38**, 313 (1982).
Naidu, D. V. P., R. Rajan, R. Kumar, K. S. Gandhi, V. H. Arakeri, and S. Chandrasekharan, "Modeling of Batch Sonochemical Reactor," *Chem. Eng. Sci.*, **49**, 877 (1994).
Pierce, A. D., *Acoustics: An Introduction to Its Physical Principals and Applications*, Acoustical Society of America, New York (1989).
Plesset, M. S., "Dynamics of Cavitating Bubbles," *J. Appl. Mech. Trans. ASME*, **16**, 277 (1949).
Plesset, M. S., and S. A. Zwick, "A Nonsteady Heat Diffusion Problem with Spherical Symmetry," *J. Appl. Phys.*, **23**, 95 (1952).
Press, W. H., S. A. Teukolsky, W. T. Vetterling, and B. P. Flannery, *Numerical Recipes*, Cambridge Univ. Press, Cambridge (1992).
Prosperetti, A., K. W. Commander, and L. A. Crum, "Nonlinear Bubble Dynamics," *J. Acoust. Soc. Amer.*, **83**, 502 (1986).
Prospreretti, A., and K. W. Commander, "Linear Pressure Waves in Bubbly Liquids: Comparison Between Theory and Experiment," *J. Acoust. Soc. Amer.*, **85**(2), 732 (1989).
Rathi, N. H., G. N. Mock, R. E. McCall, and P. L. Grady, "Ultrasound Aided Open Width Washing of Mercerized 100% Cotton Twill Fabric," *AATCC Book of Papers*, Amer. Assoc. Textile Chemists and Colorists, p. 254 (1997).
Rayleigh, Lord, "On the Pressure Developed in a Liquid During the Collapse of Spherical Cavity," *Philos. Mag.*, **34**, 94 (1917).
Safar, M. H., "Comments on Papers Concerning Rectified Diffusion of Cavitation Bubbles," *J. Acoust. Soc. Amer.*, **43**, 1188 (1968).
Shah, Y. T., A. B. Pandit, and V. S. Moholkar, *Cavitation Reaction Engineering*, Plenum Press, New York (1999).
Silberman, E., "Sound Velocity and Attenuation in Bubble Mixtures Measured in Standing Wave Tubes," *J. Acoust. Soc. Amer.*, **27**, 534 (1955).
Thakore, K. A., "Physico-Chemical Study on Applying Ultrasonics in Textile Dyeing," *Amer. Dyestuff Rep.*, **79**(5), 45 (1990).
Van Wijngaarden, L., "On the Equations of Motion For Mixtures of Liquid and Gas Bubbles," *J. Fluid Mech.*, **33**, 465 (1968).
van Wijngaarden, L., "One-Dimensional Flow of Liquids Containing Small Gas Bubbles," *Annu. Rev. Fluid Mech.*, **4**, 369 (1972).
Van der, Vlist, P., M. M. C. G Warmoeskerken, and S. Willemse, European Patent No. EP9401241 (1994).
Yachmenev, V. G., E. J. Blanchard, and A. H. Lambert, "Study of the Influence of Ultrasound on Enzymatic Treatment of Cotton Fabric," *Text. Color. Chem. & Amer. Dyestuff Rep.*, **1**(1), 47 (1999).
Young, F. R., *Cavitation*, McGraw-Hill, London (1989).

Manuscript received Sept. 16, 2002, and revision received Mar. 15, 2003.